






A new interpretation of the absorption and the dual fluorescence of Prodan in solution

Cite as: J. Chem. Phys. **153**, 244104 (2020); <https://doi.org/10.1063/5.0025013>

Submitted: 12 August 2020 . Accepted: 29 November 2020 . Published Online: 22 December 2020

 Cíntia C. Vequi-Suplicy,  Yoelvis Orozco-Gonzalez,  M. Teresa Lamy,  Sylvio Canuto, and  Kaline Coutinho

COLLECTIONS

Paper published as part of the special topic on [Special Collection in Honor of Women in Chemical Physics and Physical ChemistryWCP2020](#)



View Online



Export Citation



CrossMark

ARTICLES YOU MAY BE INTERESTED IN

[Directing excited state dynamics via chemical substitution: A systematic study of \$\pi\$ -donors and \$\pi\$ -acceptors at a carbon-carbon double bond](#)

The Journal of Chemical Physics **153**, 244307 (2020); <https://doi.org/10.1063/5.0031689>

[Excited state diabatization on the cheap using DFT: Photoinduced electron and hole transfer](#)

The Journal of Chemical Physics **153**, 244111 (2020); <https://doi.org/10.1063/5.0035593>

[Photoexcitation dynamics in perylene diimide dimers](#)

The Journal of Chemical Physics **153**, 244117 (2020); <https://doi.org/10.1063/5.0031485>



Your Qubits. Measured.

Meet the next generation of quantum analyzers

- Readout for up to 64 qubits
- Operation at up to 8.5 GHz, mixer-calibration-free
- Signal optimization with minimal latency

[Find out more](#)



A new interpretation of the absorption and the dual fluorescence of Prodan in solution

Cite as: J. Chem. Phys. 153, 244104 (2020); doi: 10.1063/5.0025013

Submitted: 12 August 2020 • Accepted: 29 November 2020 •

Published Online: 22 December 2020



View Online



Export Citation



CrossMark

Cíntia C. Vequi-Suplicy,^{1,2} Yoelvis Orozco-Gonzalez,^{1,3} M. Teresa Lamy,¹ Sylvio Canuto,¹ and Kaline Coutinho^{1,a)}

AFFILIATIONS

¹Instituto de Física, Universidade de São Paulo, Rua do Matão, 1371, 05508-090 São Paulo, SP, Brazil

²Fundacion IMDEA-Nanociencia Cantoblanco, 28049 Madrid, Spain

³Department of Chemistry, Georgia State University, Atlanta, Georgia 30302, USA

Note: This paper is part of the JCP Special Collection in Honor of Women in Chemical Physics and Physical Chemistry.

a) Permanent address: Instituto de Física, Universidade de São Paulo, Rua do Matão 1371, Cidade Universitária, 05508-090 São Paulo, SP, Brazil. **Author to whom correspondence should be addressed:** kaline@if.usp.br. Tel.: +55 11 3091 6745

ABSTRACT

Remarkable interest is associated with the interpretation of the Prodan fluorescent spectrum. A sequential hybrid Quantum Mechanics/Molecular Mechanics method was used to establish that the fluorescent emission occurs from two different excited states, resulting in a broad asymmetric emission spectrum. The absorption spectra in several solvents were measured and calculated using different theoretical models presenting excellent agreement. All theoretical models [semiempirical, time dependent density functional theory and second-order multiconfigurational perturbation theory] agree that the first observed band at the absorption spectrum in solution is composed of three electronic excitations very close in energy. Then, the electronic excitation around 340 nm–360 nm may populate the first three excited states (π - π^* L_b, n - π^* , and π - π^* L_a). The ground state S₀ and the first three excited states were analyzed using multi-configurational calculations. The corresponding equilibrium geometries are all planar in vacuum. Considering the solvent effects in the electronic structure of the solute and in the solvent relaxation around the solute, it was identified that these three excited states can change the relative order depending on the solvent polarity, and following the minimum path energy, internal conversions may occur. A consistent explanation of the experimental data is obtained with the conclusive interpretation that the two bands observed in the fluorescent spectrum of Prodan, in several solvents, are due to the emission from two independent states. Our results indicate that these are the n - π^* S₂ state with a small dipole moment at a lower emission energy and the π - π^* L_b S₁ state with large dipole moment at a higher emission energy.

Published under license by AIP Publishing. <https://doi.org/10.1063/5.0025013>

I. INTRODUCTION

Prodan (2-dimethylamino-6-propionynaphthalene, Fig. 1) and its derivatives, such as Laurdan, are widely used in biologically relevant systems^{1–7} as fluorescent probes. It is very sensitive to the environment with its remarkable emission spectrum shifting by about 120 nm ($6.4 \times 10^3 \text{ cm}^{-1} = 0.79 \text{ eV}$) from cyclohexane ($\lambda_{max} = 400 \text{ nm} = 25.5 \times 10^3 \text{ cm}^{-1} = 3.16 \text{ eV}$) to water ($\lambda_{max} = 520 \text{ nm} = 19.1 \times 10^3 \text{ cm}^{-1} = 2.37 \text{ eV}$).^{1,8–10} Inserted in biological membranes, its emission spectra depend on the lipid bilayer phase (gel or fluid),

with the wavelength of the maximum of the spectrum shifting by 50 nm ($2.4 \times 10^3 \text{ cm}^{-1} = 0.30 \text{ eV}$) from one phase to the other.^{3,7,11}

The emission spectrum of Prodan is very peculiar because it is broad and asymmetric and is composed by dual emission in several distinct environments from nonpolar to polar solutions^{12–15} and also in biological systems.^{7,11,16} The explanation for these dual emissions is still a matter of discussion.^{17–20} The common hypothesis is that the dual fluorescence comes from only one electronic state, the first excited state S₁, but with a higher emission energy coming from a solvent-non-relaxed S₁ state, the so-called locally excited (LE) state,

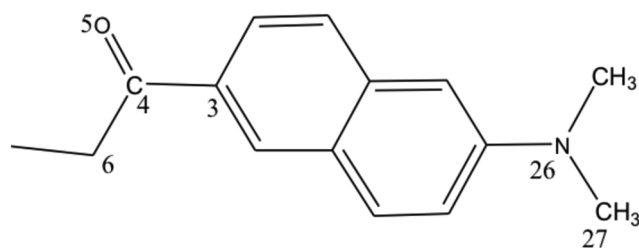
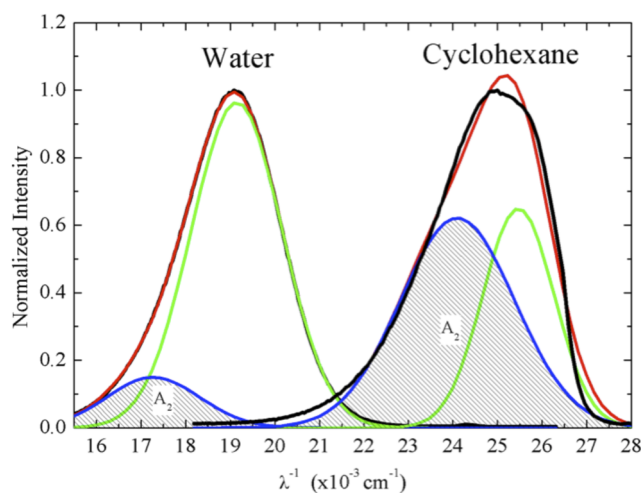


FIG. 1. Prodan molecular structure.

and another with a lower emission energy coming from a solvent-relaxed S_1 state, the so-called internal charge transfer (ICT) state, possibly also with an internal twist of the fluorophore (TICT).^{21–37} Other studies recognize some limitations of this hypothesis, suggesting that more investigation is necessary to fully understand the dual fluorescence of Prodan.^{8,10,14–19,36,38} Therefore, understanding the origin of the dual emission decay mechanism is critical to improve the applications of Prodan and its derivative as fluorescent probes in biological environments.

It is important to note two consequences of this common hypothesis of the dual emission of Prodan due to the solvent-non-relaxed S_1 state (higher emission energy E_1 or λ_1^{-1} , locally excited state) and the solvent-relaxed S_1 state (lower emission energy E_2 or λ_2^{-1} , charge transfer excited state): (i) as the difference between the two emitting states comes from the solute–solvent relaxation during the emission process, one should expect a temperature dependence of the emission spectrum shape due to the different kinetic energy, which induces a faster relaxation and consequently an increase in the fraction of the lower energy emission de-excitation with the increase in temperature (increasing temperature \rightarrow increasing E_2^{exp} intensity or area), and (ii) as the relaxed S_1 state is considered to be a charge transfer excited state, one should expect a larger dipole moment that induces a better stabilization in polar solvents and consequently an increase in the fraction of the lower energy emission de-excitation with the increase in solvent polarity (increasing polarity \rightarrow increasing E_2^{exp} intensity or area). None of these dependencies were observed experimentally. Indeed, the behavior of the dual emission of Prodan (also its derivative Laurdan) was analyzed with respect to the temperature and the solvent polarity variations in an experimental study.¹⁰ The temperature was changed from 5 °C to 40 °C, and no difference was observed in either the emission spectra of Prodan or Laurdan (experimental observation: increasing temperature \rightarrow no change in E_1^{exp} and E_2^{exp}). This experimental information contradicts the first consequence of the common hypothesis discussed above. Additionally, the effect of solvent polarity was analyzed with two different and independent techniques used to decompose the emission spectra: the decomposition into two Gaussian bands and the decay associated spectra methodology using time resolved fluorescence. The maxima of the higher energy emission band of Prodan in several solvents were measured, $E_1^{\text{exp}} = 25.5, 23.1, 22.9, 21.4, 20.1,$ and $19.1 \times 10^3 \text{ cm}^{-1}$ ($\lambda_1^{\text{exp}} = 393 \text{ nm}, 433 \text{ nm}, 437 \text{ nm}, 467 \text{ nm}, 496 \text{ nm},$ and 522 nm) for cyclohexane, chloroform, dichloromethane, acetonitrile, methanol, and water, respectively, and for the lower energy emission band in the same solvents, they were measured, $E_2^{\text{exp}} = 24.1, 21.8, 21.5, 20.3, 18.9,$ and

$17.3 \times 10^3 \text{ cm}^{-1}$ ($\lambda_2^{\text{exp}} = 415 \text{ nm}, 459 \text{ nm}, 466 \text{ nm}, 493 \text{ nm}, 528 \text{ nm},$ and 579 nm), respectively. Both emission bands are red shifted by increasing the polarity of the solvent from cyclohexane to water (experimental observation: increasing polarity ΔE_1 and ΔE_2 are red shifted). These information can be shown in Fig. 2 where the experimental fluorescent emission spectra of Prodan in cyclohexane and water solutions, obtained in previous work,¹⁰ are shown together with the two decomposed bands for each solvent. Comparing the maximum intensity of these two decomposed bands, E_1^{exp} and E_2^{exp} , and the band areas, it was obtained that the fraction of the lower energy band is higher in cyclohexane than in water, decreasing as the polarity of the solution increases, i.e., the intensities are 0.62, 0.54, 0.46, 0.34, 0.24, and 0.15 for the solvents, respectively, and the area fractions are $A_2/A_T = 61\%, 52\%, 43\%, 36\%, 26\%$, and 14% , respectively.¹⁰ Therefore, the lower energy E_2^{exp} emission is disfavored as the solvent polarity increases, i.e., the amount of photons emitted from the lower energy excited state is smaller in water than in cyclohexane. This finding is in agreement with the previous study performed in the ethanol/water mixture¹⁴ and ethanol/buffer mixture.¹⁵ However, it is in conflict with the second consequence of the common hypothesis discussed above. Therefore, a new hypothesis for the dual fluorescence of Prodan (and Laurdan) in homogeneous solvents is possible, where the two emission bands would come from two different excited electronic states,^{10,14,15} where the lower energy E_2 emission state should have a small dipole moment (because this state is disfavored with increasing polarity) and the higher energy E_1 emission state should have a large dipole moment (because this state is favored with increasing polarity). To verify this possibility or suggest a new one, Monte Carlo (MC) and Molecular Dynamics (MD) simulations and quantum mechanics calculations were performed in this work, along with experimental measures of the Prodan spectrum in different solvents. The low-lying excited electronic states

FIG. 2. Experimental fluorescent emission spectra of Prodan in cyclohexane and water solutions (in black). Gaussian decomposition: higher energy E_1 or λ_1^{-1} band (in green), lower energy E_2 or λ_2^{-1} band (in blue), and total band (in red). Data obtained from Ref. 10.

and deactivation mechanisms of Prodan were characterized in vacuum and in solvents, and also, the absorption and emission spectra were computed.

Initially, the electronic transition energies of Prodan in some solvents were calculated and compared with the experimental data of the first band of the UV–visible absorption spectra. This motivated us to obtain again the experimental absorption spectrum and analyze also the broadening of the band. An excellent agreement was found between the theoretical results and the experimental data, and the important conclusion obtained from this comparison was the existence of three electronic excitations in the first absorption band. Therefore, by exciting Prodan at the wavelength of the maximum absorption of the first band, our calculations show that it is possible to populate three different excited states. These combined theoretical and experimental results along with the characterization of the low-lying excited electronic states of the Prodan will be used to support the hypothesis that Prodan fluorescent emission is due to the decay of two independent states that are accessible in the absorption band and can be populated when Prodan is excited with energies around $27.8\text{--}29.5 \times 10^3 \text{ cm}^{-1}$ (360 nm–340 nm). These two states are characterized with quantum mechanics (QM) calculations using different theoretical levels ranging from semi-empirical to multi-configurational perturbation theory.

II. EXPERIMENT

To assist and complement our theoretical results for the absorption spectra of Prodan in different solvents, these spectra were measured experimentally in this work.

A. Materials and methods

The fluorophores Prodan and Laurdan were purchased from Molecular Probes Inc. (Eugene, OR, USA) and the solvents cyclohexane, chloroform, dichloromethane, acetonitrile, and methanol from Sigma-Aldrich (St Louis, MO, USA). Water was Milli-Q Plus (Millipore), pH ~ 6.0 . Stock solutions of the fluorophore in chloroform (1.5 mM) were used in all experiments. Appropriated amounts of these solutions were transferred to glass flasks using calibrated glass microsyringes. Chloroform was evaporated under a stream of dry N_2 . The dry residue was dissolved in the desired solvent to obtain the fluorophore concentration of $4.0 \mu\text{M}$. pH was measured for all samples in water, and no change was observed (pH ~ 6.0).

The electronic absorption spectra were measured with a Cary-50 spectrophotometer (Varian Australia PTY Ltd., Mulgrave, VIC, Australia) with the temperature fixed at $25^\circ\text{C} \pm 1^\circ\text{C}$ with a single cell Peltier temperature controller. All data shown are averages of at least three experiments.

III. COMPUTATIONAL DETAILS

A. Solute polarization in solution

The solvent effects in the electronic states (ground and excited states) and in the transition energies were taken into account using the sequential Quantum Mechanics/Molecular Mechanics (S-QM/MM) methodology,^{39–41} unless the polarizable continuum model (PCM)⁴² were stated.

The S-QM/MM methodology is a two steps procedure: first, MM simulations were performed considering the solute surrounded by the solvent in a specific thermodynamic condition, and then, QM calculations were performed in solute–solvent configurations obtained from the MM simulations to provide averaged electronic properties. Usually, after the simulations, a statistical analysis is performed³⁹ and 100 statistically uncorrelated solute–solvent configurations (less than 10% of statistical correlation) were selected and submitted to QM calculations to obtain averaged solute electronic properties at a specific thermodynamic condition. This procedure was successfully used for several properties such as solute polarization,^{39,43} UV–vis absorption spectrum,^{40,41,44,45} and nuclear magnetic resonance (NMR) properties,⁴⁶ where the solvent was used in the QM calculations either as electrostatic embedding only or in addition to some closer explicit solvent molecules. For the cases where the solvent effect is treated only by the electrostatic embedding, we have shown that the average of 100 QM calculations can be represented by one QM calculation performed with the Average Solvent Electrostatic Configuration (ASEC).⁴⁷ This makes it possible to compute properties of the excited electronic states in a very efficient way considering the effect of the environment.

The solute polarization was obtained using the ASEC in an iterative-QM/MM polarization procedure.^{44–47} The iteration starts with a MM simulation of the solute–solvent system where the classical electrostatic potential uses atomic charges of the solute obtained from the QM calculation in vacuum or from a previous PCM calculation. Then, after the simulations, the solvent distribution around the solute is obtained to generate the ASEC, and a new QM calculation is performed, recalculating new solute atomic charges to start a following iteration step. This procedure is repeated several times until reaching converged atomic charges or dipole moment. In the case of Prodan, we obtained the atomic charges with the CHELPG procedure⁴⁸ for the electrostatic fitting calculated at the MP2/aug-cc-pVDZ level for the ground state and with the Electrostatic Potential Fitted method (ESPF)⁴⁹ at the CASSCF/ANO-L level for the ground and excited states. Then, for both QM levels (MP2 and CASSCF), an ASEC electrostatic embedding of the solvent was used to include the electronic polarization of the solute ground state (S_0) in different solvents. Also, the iterative polarization procedure was performed for the first three excited electronic states ($\pi\text{--}\pi^*L_a$, $\pi\text{--}\pi^*L_b$, and $n\text{--}\pi^*$) only with CASSCF to obtain the Prodan electron density in electrostatic equilibrium with the water solution, as performed before.^{44–47,50} It is important to note that this polarization procedure allows the relaxation of the electronic density of the solute in the presence of the solvent. Therefore, when the polarizations of the excited states are performed at the S_0 geometry, the instantaneous relaxed electronic state in solution is obtained to describe the vertical excitation. However, when the polarizations are performed at the corresponding equilibrium excited state geometry, the fully relaxed electronic state in the solution is obtained to describe the emission transition. Here, as the excited states geometries of Prodan were optimized in vacuum, the solvent effect in the geometry relaxation was not taken into account. However, to consider this geometry relaxation solvent effect, it is necessary to analyze the possibility of new force field parameters to avoid the bias and properly describe the equilibrium excited state geometries in the MM simulations.

B. Absorption and emission spectra

The absorption spectra were calculated using four different methods: (1) Time Dependent Density Functional Theory (TD-DFT)⁵¹ using the B3LYP functional and 6-311G(d) basis set with the solvent treated as the polarizable continuum model (PCM).⁴² This method will be called TD-B3LYP/PCM; (2) semi-empirical Intermediate Neglect of Differential Overlap with single excitations in the Configuration Interaction method (INDO-CIS) using the original spectroscopic parameterization⁵² with the solvent included as the Self-Consistent Reaction Field (SCRF).^{53,54} This method will be called INDO-CIS/SCRF; (3) semi-empirical INDO-CIS with the solvent included as explicit molecules using solute-solvent configurations obtained from the molecular mechanics simulation with either methods: Molecular Dynamics (MD) or Monte Carlo (MC). This method will be called INDO-CIS/explicit. It uses several solute-solvent configurations characterizing the solution at a specific thermodynamic condition. Then, naturally, it provides inhomogeneous contribution to the band broadening. The details of the simulations are given below; (4) single-state second order multi-configurational perturbation theory (CASPT2)⁵⁵ based on a multi-state Complete Active Space Self-Consistent Field (CASSCF) wave function.⁵⁶ This method was used to compute the absorption spectrum of the Prodan, but also to characterize the low-lying excited electronic states and compute the emission spectrum, both in vacuum and in water solution treated with PCM and with ASEC electrostatic embedding. This method will be called CASPT2/PCM and CASPT2/ASEC. The active space of CASSCF calculations correlates 12 electrons in 12 orbitals, termed CASSCF(12, 12). The active orbitals are the five π and six π^* that better describe the two lowest π - π^* excited states, and the oxygen lone-pair orbital was added to describe the lowest n - π^* excited state. The ANO-L basis set^{57,58} was used with the contraction scheme C, O and N (14s9p4d)/[4s3p1d], H (8s4p)/[2s1p]. The ground and excited electronic states were optimized at the same level using CASSCF/ANO-L-4s3p1d/2s1p in vacuum. The vibration frequencies were also calculated to ensure the equilibrium geometry of each state, and the total energy was corrected by the zero-point energy and vibrational entropy.

The ground state equilibrium geometry of the Prodan was previously obtained by Vequi-Suplicy *et al.*⁴⁵ This planar geometry, generated with the DFT/B3LYP/6-31G(d) level, does not show significant changes when optimized in vacuum or in solution (treated as PCM). This behavior persisted even using two additional basis sets [6-311+G(d) and aug-cc-pVDZ]. For comparison with the previous result, this geometry was also used in the calculation of the absorption spectrum of Prodan in solution with three methods: TD-B3LYP/PCM, INDO-CIS/SCRF, and INDO-CIS/Explicit.

All the semi-empirical calculations were performed with the ZINDO program,⁵⁹ the DFT calculations were performed with the Gaussian03 program package,⁶⁰ and the multi-configurational calculations were performed with the MOLCAS 7.6 program package.⁶¹

C. Molecular mechanics simulations

The Molecular Mechanics simulations were performed using the standard Monte Carlo (MC) method with the Metropolis sampling technique⁶² with the solute rigid in the optimized geometry.

Nevertheless, to take into account the effect of the intramolecular degree of freedom, Molecular Dynamics (MD) was also performed. The MD flexibility is expected to mostly affect the C=O stretch in water due to the formation of hydrogen bonds (HBs) and possible rotations between the aromatic ring and the other groups. The isothermal-isobaric *NPT* ensemble at room temperature and pressure conditions (298 K and 1 atm) was used in both the MC and MD simulations. One Prodan and 1000 water molecules or 500 molecules of the other solvents (acetonitrile, dichloromethane, and cyclohexane) were considered in a rectangular box with periodic boundary conditions and minimum image method. The intramolecular parameters of Prodan used in flexible simulation were obtained from the all-atom Optimized Potentials for Liquid Simulations (OPLS/AA) force field.⁶³ However, the equilibrium bond distances and angles were used from the optimized geometry with QM calculation with the B3LYP/6-31G(d) level and the rotational angles between the aromatic rings and the $-N(CH_3)_2$ and the $-COCH_2CH_3$ groups ($\varphi_{O-C-C-C}$, $\varphi_{C-N-C-C}$, and $\varphi_{H-C-N-C}$) were reparametrized to describe QM energy profile with the same level. The intermolecular interactions were described by the Lennard-Jones plus Coulomb potentials with three parameters for each interacting site (ϵ_i , σ_i , and q_i for an atom i). The Lennard-Jones, ϵ_i and σ_i , parameters for the Prodan were obtained from the all-atom Optimized Potentials for Liquid Simulations (OPLS/AA) force field,⁶³ and the atomic charges, q_i , of the Coulomb potential were obtained with QM calculations polarized in the presence of the solvent with an iterative-QM/MM polarization procedure,⁴⁴⁻⁴⁷ as discussed in Sec. III A.

The geometry and the parameters used for the solvents were the simple point charge model (SPC/E)⁶⁴ for water, the parameters of Bohm *et al.*⁶⁵ for acetonitrile, and the OPLS-AA⁶³ for dichloromethane and cyclohexane in the chair conformation.

The MC simulation consisted of a thermalization stage of 1.2×10^8 MC steps, followed by an equilibrium stage of 1.5×10^8 MC steps, where in each step, one molecule was randomly selected to translate and rotate according to the Metropolis sampling technique. A thermalized configuration obtained from the MC simulation was used to start the MD simulations. A thermalization phase of 3 ns was performed to equilibrate the kinetic and potential energy, and the MD simulation was carried out for 6 ns more. The time step was 0.1 fs. To solve the equations of motion, the integrator method was the velocity-Verlet.⁶⁶ To keep the temperature and pressure constant, the Berendsen thermostat and barostat were used.⁶⁷ All the MC simulations were performed with the DICE program,^{68,69} and the MD was performed using the TINKER program.^{70,71}

After the simulations, 100 statistically uncorrelated configurations of the solute-solvent system were selected and submitted to QM calculations of the absorption energies. The configurations selected for the QM calculation were composed by one Prodan molecule, the first solvation shell as explicit solvent molecules, and the second solvation shell treated as an electrostatic embedding using the atomic charges of the solvent molecules (obtained from the classical force field). The calculations were first performed using the semi-empirical INDO-CIS method considering all occupied and unoccupied valence orbitals, i.e., a full CIS considering 43 occupied orbitals and 44 unoccupied. Another set of QM calculations was performed with 100 statistically uncorrelated configurations to

generate ASEC where all solvent molecules are treated as an electrostatic embedding described by atomic point charges.

IV. RESULTS AND DISCUSSIONS

A. Geometry, polarization, and solvation

The optimized geometry of Prodan in the ground state S_0 obtained with the B3LYP/6-31G(d) method is a planar structure with a small bending of the methyl groups bonded to the nitrogen atom ($\varphi_{C-N-CH_3-CH_3} = 165.3^\circ$), in good agreement with the x-ray crystallographic structure.³⁰ The calculated value of the dipole moment is 5.8 D in vacuum with MP2/aug-cc-pVDZ (see Table I). In the solvent environment, the electronic state relaxes due to the solvent interaction, and the dipole moment increases to 6.1 D, 7.7 D, 8.0 D, and 10.2 D in cyclohexane, dichloromethane, acetonitrile, and water, respectively, as discussed before⁴³ using the iterative-QM/MM procedure with MP2/aug-cc-pVDZ. The polarization of Prodan in solution increases with the solvent polarity, and the effect of the water is remarkable with an increase of 176%. Analyzing the charge distribution of the Prodan in vacuum (non-polarization), there is a small charge separation between the electron donor and acceptor groups [$q_i(N)-q_i(O) = 0.16 e$] but a large local charge separation in the C=O bond [$q_i(C)-q_i(O) = 0.80 e$]. In solution, the charge separation between the electron donor and acceptor groups increases with the solvent polarity [$q_i(N)-q_i(O) = 0.25, 0.30, 0.26,$ and $0.47 e$ for cyclohexane, dichloromethane, acetonitrile, and water, respectively], and the local charge separation in the C=O bond increases even more [$q_i(C)-q_i(O) = 0.99, 1.10, 1.06,$ and $1.36 e$, respectively]. The electronic distribution of Prodan is very sensitive to the environment and hence subjected to considerable polarization.

The geometry of the ground state S_0 obtained with CASSCF/ANO-L in vacuum is similar to the one optimized with the B3LYP/6-31G(d) method discussed above. The vertical excited states (in the S_0 equilibrium geometry) $\pi-\pi^*L_b$, $n-\pi^*$, and $\pi-\pi^*L_a$ are close in energy, within 0.3 eV ($2.2 \times 10^3 \text{ cm}^{-1}$), but they have quite different electronic structure that leads to the dipole moments of 5.7,

1.5, and 11.4D, respectively, in vacuum. Therefore, comparing their dipole moment with the ground state S_0 (5.3D), the $\pi-\pi^*L_b$ state has a similar value, the $n-\pi^*$ state has a much smaller value, and the $\pi-\pi^*L_a$ state has a much larger value. These three excited states relax to their equilibrium geometry, stabilizing by 0.3 eV, 1.2 eV, and 0.7 eV, respectively. The geometry differences of the relaxed low-lying excited states in vacuum compared to the ground state are small, mostly the planarity of the amino group and the C=O distance. The $\pi-\pi^*L_b$, $n-\pi^*$, and $\pi-\pi^*L_a$ equilibrium geometries are fully planar, i.e., with a planar improper dihedral angle between the methyl groups bonded to the nitrogen atom and the aromatic rings, $\varphi_{C-N-CH_3-CH_3} = 179^\circ$ for $\pi-\pi^*L_b$ and 180° for $n-\pi^*$ and $\pi-\pi^*L_a$. Moreover, the C=O distances are $d_{CO} = 1.225 \text{ \AA}$ for S_0 , 1.210 \AA for $\pi-\pi^*L_b$, 1.357 \AA for $n-\pi^*$, and 1.216 \AA for $\pi-\pi^*L_a$. Additionally, for the $n-\pi^*$ geometry, there are variations of the related angles, such as $\theta_{O-C-CH_3} = 120^\circ$ for S_0 , $\pi-\pi^*L_b$, and $\pi-\pi^*L_a$ and 113° for $n-\pi^*$. The main difference between the equilibrium geometry of the $\pi-\pi^*L_a$ and $\pi-\pi^*L_b$ is a small reduction in the distance of the nitrogen atom and the carbon of the rings, $d_{NC} = 1.385 \text{ \AA}$ for $\pi-\pi^*L_a$ and 1.339 \AA for $\pi-\pi^*L_b$. All the Cartesian coordinates of the four equilibrium geometries (S_0 , $\pi-\pi^*L_b$, $n-\pi^*$, and $\pi-\pi^*L_a$) are presented in the supplementary material.

The geometry optimizations and the minimum energy path (MEP) for the three low-lying excited states were performed also in geometries with rotations at the $-N(CH_3)_2$ and $-COCH_2CH_3$ groups. However, in vacuum, the planar geometries were found to be the most stables with lower energies.

Using the equilibrium geometry for each one of the four electronic states of Prodan, the charge distribution was calculated in vacuum and in aqueous solution with CASSCF/ANO-L/ESPF using the iterative-QM/MM procedure with ASEC. The calculated values of the dipole moment in vacuum are $\mu_{vac}(S_0) = 5.3 \text{ D}$, $\mu_{vac}(\pi-\pi^*L_b) = 5.8 \text{ D}$, $\mu_{vac}(n-\pi^*) = 1.6 \text{ D}$, and $\mu_{vac}(\pi-\pi^*L_a) = 11.2 \text{ D}$ (see Table I). Therefore, the relaxation to the equilibrium geometry has only a small effect in the dipole moment of the excited states compared with the vertically excited states (in the S_0 geometry). On the other hand, the solvent effect is considerable. Their fully relaxed dipole moments in water are $\mu_{wat}(S_0) = 9.1 \text{ D}$, $\mu_{wat}(\pi-\pi^*L_b) = 9.7 \text{ D}$,

TABLE I. The atomic charges (in e) of some atoms, C=O and N, and the dipole moment (in D) of Prodan in vacuum and in aqueous solution are shown. The values are calculated for the ground state (S_0) and for the three low-lying relaxed excited states ($\pi-\pi^*L_b$, $n-\pi^*$, and $\pi-\pi^*L_a$) with CASSCF/ANO-L/ESPF. The values for the vertical excited states are shown in parentheses. For comparison, the atomic charges of the S_0 were also calculated with MP2/aug-cc-pVDZ/CHELPG.

	S_0 (MP2)	S_0 (CASSCF)	$\pi-\pi^*L_b$ (CASSCF)	$n-\pi^*$ (CASSCF)	$\pi-\pi^*L_a$ (CASSCF)
Vacuum					
$q_i(C)$	0.36	0.34	0.48	0.04	0.37
$q_i(O)$	-0.44	-0.42	-0.59	-0.15	-0.52
$q_i(N)$	-0.28	-0.18	-0.07	-0.03	-0.03
μ	5.8	5.3	5.8(5.7)	1.6(1.5)	11.2(11.4)
In water					
$q_i(C)$	0.60	0.86	0.66	-0.10	0.45
$q_i(O)$	-0.76	-0.88	-0.87	-0.22	-0.89
$q_i(N)$	-0.29	-0.09	-0.05	-0.21	-0.17
μ	10.2	9.1	9.7(9.7)	2.7(4.8)	17.2(17.9)

$\mu_{\text{wat}}(n-\pi^*) = 2.7$, and $\mu_{\text{wat}}(\pi-\pi^*L_a) = 17.2$ D. The electronic polarization of the Prodan in water is remarkable with an increase in the dipole moment of 160% in the S_0 , 167% at $\pi-\pi^*L_b$, 181% in the $n-\pi^*$, and 154% in the $\pi-\pi^*L_a$, considering the relaxed equilibrium geometry of each state optimized in vacuum. These dipole moment values are also presented in [Table I](#) together with some relevant atomic charges. The complete sets of atomic charges (in vacuum and polarized in water) are presented in the [supplementary material](#), together with the dipole moment evolutions during the iterative-QM/MM polarization procedure.

Comparing the ground state S_0 with the $\pi-\pi^*L_b$, $n-\pi^*$ and $\pi-\pi^*L_a$ excited states, it was found that the $\pi-\pi^*L_b$ state has a dipole moment slightly larger than the S_0 [$\mu_{\text{wat}}(S_0) = 9.1$ D and $\mu_{\text{wat}}(\pi-\pi^*L_b) = 9.7$ D], but the $n-\pi^*$ state has a large decrease [$\mu_{\text{wat}}(n-\pi^*) = 2.7$ D], and the $\pi-\pi^*L_a$ state has a large increase [$\mu_{\text{wat}}(\pi-\pi^*L_a) = 17.2$ D].

Recently, Baral *et al.*⁷² studied the relaxation of the first excited state S_1 (HOMO \rightarrow LUMO) of Prodan in several solvents (hexane, acetone, octanol, ethanol, methanol, and water) using a theoretical procedure and ultrafast time-resolved transient absorption measurements. Comparing the Prodan molecular orbital calculated by them and by us, we identified that the reported S_1 state is the $\pi-\pi^*L_a$ state (see the discussion about the excited states in [Sec. IV C](#)). They used an iterative-QM/MM procedure, similar to ours, where the QM calculations are performed with many-body Green functions within the GW approximation and the Bethe–Salpeter equation (GW-BSE). The MM simulations were made with the MD simulations, recalculating the atomic charges of the Prodan at the S_1 state with electrostatic embedding in each iterative step. In hexane, they obtained the vertical non-relaxed dipole moment of 5.50 D and the fully relaxed $\mu_{\text{hex}}(S_1) = 10.98$ D, and in water, the vertical non-relaxed moment is ~ 9 D and the fully relaxed $\mu_{\text{hex}}(S_1)$ moment is ~ 24 D, showing a remarkable polarization and relaxation effects of the Prodan S_1 around 200% in hexane and 266% in water. These values are larger than our calculated values and the reason may come from two differences: (i) the QM methods are different, which can underestimate or overestimate the solvent interaction with the solute wavefunction and (ii) we performed the MM simulation of Prodan in solution with rigid geometry and Baral *et al.*⁷² used flexible Prodan geometry, considering the geometry relaxation due to the solvent interactions. However, since they used the same force field bonded parameters for the ground state S_0 and the first excited state S_1 , a similar geometry of both states is implicitly assumed and this is in qualitative agreement with the $\pi-\pi^*L_a$ geometry obtained in this work.

The solvation shells around Prodan are determined using the minimum distance distribution function (MDDF),^{73,74} and the effect of the polarization of the solute due to the solvent is analyzed. The MDDFs between Prodan in the ground state S_0 and the studied solvents are presented in the [supplementary material](#). For the solvents cyclohexane, dichloromethane, and acetonitrile, no significant changes were observed in the average solvation shells using the non-polarized and polarized sets of atomic charges of Prodan using MP2/aug-cc-pVDZ/CHELPG. However, for the aqueous solution, although the number of water molecules in the solvation shells remains the same, an increase in the number of hydrogen bonds was observed. The quantity of solvent molecules in the first and second solvation shells was 20 (up to 4.15 Å) and 77 (from 4.15 Å to 9.35 Å)

for cyclohexane, 24 (up to 4.65 Å) and 80 (from 4.65 Å to 8.55 Å) for dichloromethane, 29 (up to 4.15 Å) and 100 (from 4.15 Å to 7.95 Å) for acetonitrile, and 56 (up to 4.05 Å) and 231 (from 4.05 Å to 7.95 Å) for water. For the polarized Prodan in water, it is possible to observe a small peak in the MDDF around 1.70 Å that is characteristic of hydrogen bonds (HBs) between Prodan and water molecules. The number of water molecules in the solvation shells is still the same for the four electronic states, S_0 , S_1 , S_2 , and S_3 , but the number of HBs differs.

B. Absorption spectra

The experimental absorption spectra of the fluorophore Prodan and Laurdan in the six solvents are presented in [supplementary material](#). In [Fig. 3](#), only the first absorption band is shown along with the calculated excitation energies. As can be seen, this band is very broad in all solvents. Therefore, when referring to the experimental value one should consider that this is the band maximum of a considerably broad absorption band.

The results obtained with INDO-CIS/SCRF and TD-B3LYP/PCM for the first three excitations are presented as vertical lines in [Fig. 3](#). For the INDO-CIS/explicit, the excitations were calculated for 100 solute–solvent configurations obtained from the simulations. This leads naturally to band broadening, and the three calculated excitations are presented in [Fig. 3](#) as histograms, giving a very good description of the observed band. In the case of water, the solute–solvent configurations were generated with two simulation methods: MC and MD. The difference between them is the flexibility of the solute. As shown in [Fig. 3](#), the outcome of 100 QM calculations with the INDO-CIS/explicit using solute–solvent configurations obtained from the MC simulation (with rigid solute) presents a broadening caused by the diversity of solvent positions around the solute and, in the case of MD simulation, (with flexible solute) presents an even broader distribution of excitation energy due to the solute deformation. This describes very well the broadening of this first absorption band in water. Analyzing the Prodan conformations during the MD simulation, the planarity was maintained with rotational angle variations between the aromatic rings and the $-N(CH_3)_2$ and the $-COCH_2CH_3$ groups around $\pm 15^\circ$, but mostly, the deformation comes from the C=O stretch caused by the hydrogen bond formed between the Prodan and the water molecules. In cyclohexane, dichloromethane, and acetonitrile, we see the separation of the first three excitations (solid histogram in red for the $n-\pi^*$ and in blue for the $\pi-\pi^*$) of 100 solute–solvent configurations obtained with the MC simulation.

All methods used in this work agree that the first experimental band is composed of three excitations: one $n-\pi^*$ and the two $\pi-\pi^*$ transitions. In nonpolar environments (vacuum, cyclohexane, and dichloromethane), the INDO-CIS/explicit, INDO-CIS/SCRF, and the TD-B3LYP/PCM calculations show the $n-\pi^*$ as the first transition followed by the two $\pi-\pi^*$. In polar solvents (acetonitrile and water), the $n-\pi^*$ transition becomes the second excited state. This is easy to understand because in more polar solvents, the $n-\pi^*$ transition shifts to the blue (higher energy), whereas the $\pi-\pi^*$ transitions shift to the red (lower energy). This is summarized in [Table II](#). The experimental excitation energies (and wavelengths) presented at [Table II](#) correspond to the maximum

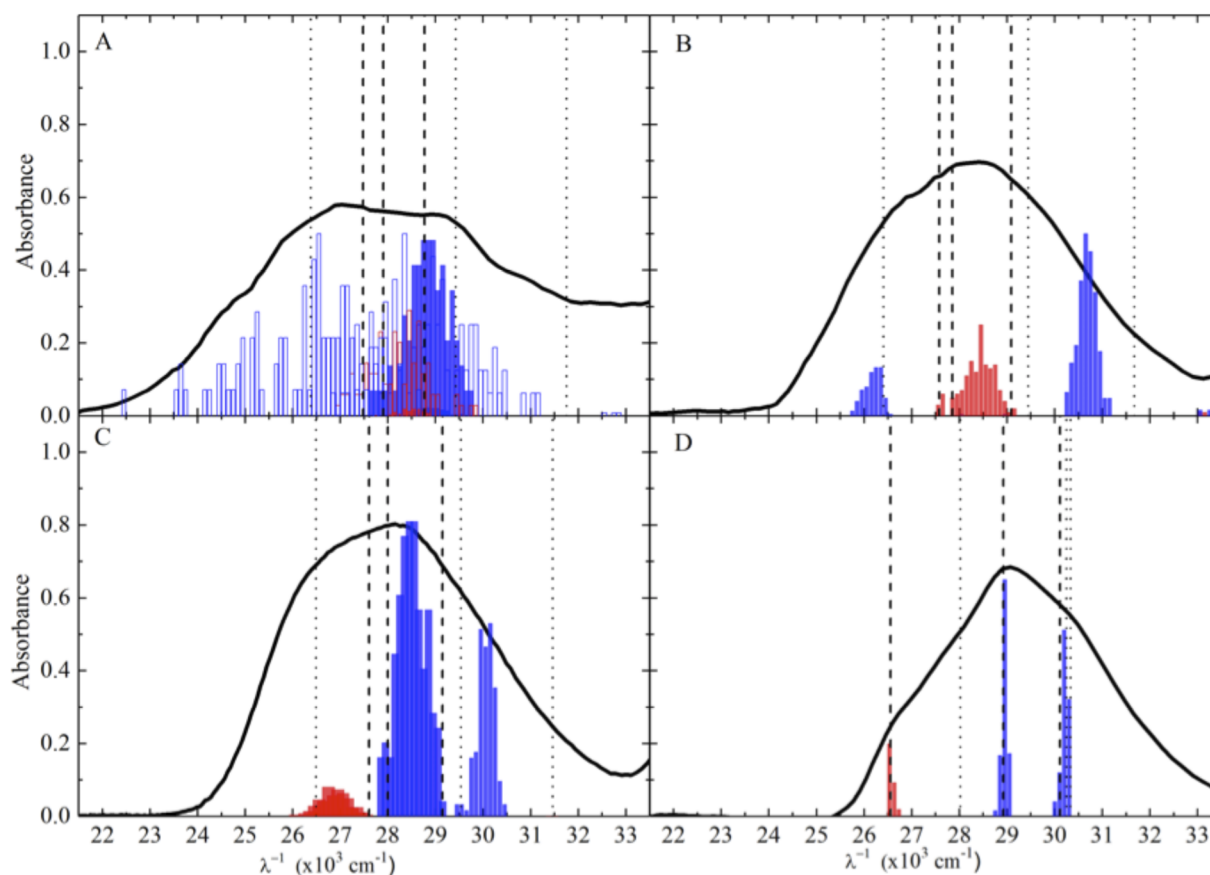


FIG. 3. Absorption spectra of Prodan in several solvents: (a) in water, (b) in acetonitrile, (c) in dichloromethane, and (d) in cyclohexane. Black solid line is the experimental result (this work). Vertical lines are the first three excitations calculated with INDO-CIS/SCRF (dashed) and B3LYP/PCM (dotted). The histograms (in red is $n-\pi^*$ and in blue is $\pi-\pi^*$ excitations) are the excitations calculated with INDO-CIS/explicit for 100 different solute-solvent configurations obtained with MC simulations for all solvent (solid histogram) and with the MD simulation (open histogram) only for water.

absorption. However, to compare with the theoretical results, it is important to consider the large broadening of this band, as shown in Fig. 3.

The excitation energies (Table II) calculated with CASPT2 are larger than those calculated with B3LYP or the two INDO-CIS models and also the experimental data. Comparing CASPT2/ASEC with B3LYP/PCM or INDO-CIS/explicit, the first $\pi-\pi^*$ excitation in water differs by 4.0 or $3.2 \times 10^3 \text{ cm}^{-1}$, respectively. In changing from vacuum to water using the CASPT2/ASEC method, the solvent shift in absorption is $-1.5 \times 10^3 \text{ cm}^{-1}$ for the first $\pi-\pi^*$ excitation, $-0.7 \times 10^3 \text{ cm}^{-1}$ for the $n-\pi^*$ excitation, and $-2.6 \times 10^3 \text{ cm}^{-1}$ for the second $\pi-\pi^*$ excitation. The experimental solvent shift going from a nonpolar solvent (cyclohexane) to a polar solvent (water) is $-1.5 \times 10^3 \text{ cm}^{-1}$. Therefore, the solvent shift of the first $\pi-\pi^*$ excitation represents the best agreement between the CASPT2/ASEC method and the experimental data. These values are comparable to the shifts obtained with the other theoretical models, shown in Table II. Despite obtaining large excitation energies, the results at the CASPT2 level agree that the first observed band should be

composed of three low-lying transitions. The separation between these three transitions amounts to $3.0 \times 10^3 \text{ cm}^{-1}$ and is still much less than the broadening experimentally observed to the first absorption band. Then, we conclude that all theoretical models adopted here agree that the first absorption band of Prodan in solution is composed by vertical excitations from the ground state to three different excited states, one $n-\pi^*$ and two $\pi-\pi^*$ states, where the first $\pi-\pi^*$ excitation represents the best agreement between theoretical and experimental solvent shift.

There are several previous studies that report theoretical results of the absorption energies of Prodan in vacuum.^{20,22,30,31,75} Most of these results underestimate the first transition and overestimate the second when compared with the results in Table II. In two previous papers,^{19,36} using the PCM model for the solvent obtained results that are in good agreement with the experimental data. Therefore, considering Fig. 3 and Table II, it is possible to conclude that the absorption spectra of Prodan in all the solvents considered are well described by three electronic excitations.

TABLE II. Calculated vertical excitation energies for Prodan in vacuum and in different solvents calculated with four different methods. In the case of the explicit solvent, the values were obtained with the average over 100 solute–solvent configurations selected from MC simulations for all solvents except for water that is from the MD simulation. The values are in 10^3 cm^{-1} and in parentheses in nm. The experimental values are the energy of the band maximum shown in Fig. 3 and obtained in this work. The asterisk indicates $n-\pi^*$ transition, in brackets indicate the CASPT2/ASEC method, and in boldface is the best agreement with the experimental energy of maximum absorption ($E_{\text{abs}}^{\text{exp}}$). The experimental values¹⁰ for the higher emission energy E_1^{exp} and lower emission energy E_2^{exp} are shown, and the Stokes shift [$\Delta E_1^{\text{exp}}(\text{SS}) = E_1^{\text{exp}} - E_{\text{abs}}^{\text{exp}}$ and $\Delta E_2^{\text{exp}}(\text{SS}) = E_2^{\text{exp}} - E_{\text{abs}}^{\text{exp}}$] are also shown.

Excitation	Vacuum	Cyclohexane	Dichloromethane	Acetonitrile	Water
Method: INDO-CIS/Explicit					
First	26.7 (375)*	26.6 ± 0.1 (376)*	26.9 ± 0.3 (372)*	26.2 ± 0.3 (382)	27.2 ± 1.2 (368)
Second	29.1 (343)	29.0 ± 0.1 (345)	28.5 ± 0.5 (351)	28.5 ± 0.5 (351)*	28.5 ± 0.7 (351)*
Third	30.0 (333)	30.2 ± 0.1 (331)	30.0 ± 0.3 (333)	30.7 ± 0.3 (326)	28.5 ± 1.1 (351)
Method: INDO-CIS/SCRF					
First	26.7 (375)*	26.9 (372)*	27.6 (362)*	27.6 (363)	27.5 (364)
Second	29.1 (343)	28.8 (347)	28.0 (357)	27.9 (359)*	27.9 (358)*
Third	30.0 (333)	30.0 (333)	29.1 (343)	29.1 (344)	28.8 (348)
Method: TD-B3LYP/PCM					
First	28.0 (370)*	27.1 (370)*	26.5 (377)*	26.4 (379)	26.4 (379)
Second	30.3 (331)	29.9 (334)	29.5 (339)	29.4 (340)*	29.4 (340)*
Third	30.3 (330)	30.8 (325)	31.5 (318)	32.0 (313)	31.7 (316)
Method: CASPT2/PCM[ASEC]					
First	31.9 (313)	30.6 (327) [30.4]
Second	32.0 (313)*	31.9 (313) [31.3]
Third	34.4 (291)	33.6 (298)* [31.8]
Absorption energy $E_{\text{abs}}^{\text{exp}}$					
		29.1 (344)	28.2 (354)	28.2 (354)	27.6 (362)
High energy emission E_1^{exp}					
		25.5 (393)	22.9 (437)	21.4 (467)	19.1 (522)
Low energy emission E_2^{exp}					
		24.1 (415)	21.5 (466)	20.3 (493)	17.3 (579)
Stokes shift $\Delta E_1^{\text{exp}}(\text{SS})$					
		−3.6	−5.3	−6.8	−8.5
Stokes shift $\Delta E_2^{\text{exp}}(\text{SS})$					
		−5.0	−6.7	−7.9	−10.3

C. The excited electronic states and the emission spectrum

To analyze the excited states of Prodan, we use the more adequate CASSCF and CASPT2 methods. The low-lying excited electronic states were first identified from the absorption transitions computed at the CASPT2 level in vacuum. Three relevant excited electronic states were identified. The $\pi-\pi^*$ state is the first $\pi-\pi^*$ electronic state in vacuum mainly described by the transitions HOMO $-1 \rightarrow$ LUMO and HOMO \rightarrow LUMO $+1$, while the $n-\pi^*$ state is characterized by the transition from the oxygen lone-pair orbital (HOMO-3) to the LUMO $+1$ and the $\pi-\pi^*$ state is mainly described by the HOMO \rightarrow LUMO transition. The molecular orbitals characterizing these electronic states are shown in Fig. 4. These orbitals are in good agreement with those obtained by Baral *et al.*⁷² using QM calculations with the GW-BSE level.

To better analyze the photophysics of Prodan in vacuum and in water solution, the energies of the ground and three excited electronic states were recalculated with the CASPT2 level using the equilibrium geometries obtained with the CASSCF(12, 12) level in vacuum. Therefore, 16 CASPT2 calculations were performed to obtain the electronic energies of four electronic states (S_0 , $\pi-\pi^*$ L_b , $n-\pi^*$, and $\pi-\pi^*$ L_a) in the equilibrium geometry of each four state obtained with CASSCF. This method will be called CASPT2//CASSCF. The

energy differences (corrected by zero-point energy and vibrational entropy) from the ground state S_0 to the excited states $\pi-\pi^*$ L_b , $n-\pi^*$, and $\pi-\pi^*$ L_a are presented in Table III, and these energy values were used to make a schematic representation of the Prodan photophysics shown in Fig. 5 [in vacuum (a) and in aqueous solution (b)]. In the x-axis, the geometries were ordered in the sequence $n-\pi^*$, $\pi-\pi^*$ L_b , S_0 , and $\pi-\pi^*$ L_a to describe the symbolic reaction coordinates. This order is arbitrary but was selected in the way to reproduce a well-behaved minimum energy profile of the ground state. In Fig. 5, the photophysics of Prodan is schematically summarized including some important energy differences presented at Table III. The gray region indicated in Fig. 5(a) shows an important characteristic of this molecular system, since excitation energies from about 31.9 to $34.2 \times 10^3 \text{ cm}^{-1}$ (292 nm–313 nm) could populate the first three excited electronic states, as they are very close in energy. In water, the excitation energies range from about 30.4 to $31.8 \times 10^3 \text{ cm}^{-1}$ (329 nm–314 nm) and also could populate the first three excited electronic states.

Taking into account that the $n-\pi^*$ excited state is a dark state due to the weak oscillator strength of the electronic transition, it is expected that the $\pi-\pi^*$ L_b and $\pi-\pi^*$ L_a states are the main populated states upon the Franck–Condon absorption transition. Following the minimum energy path (MEP) of these three states in vacuum and in water, it can be observed that internal conversions may occur.

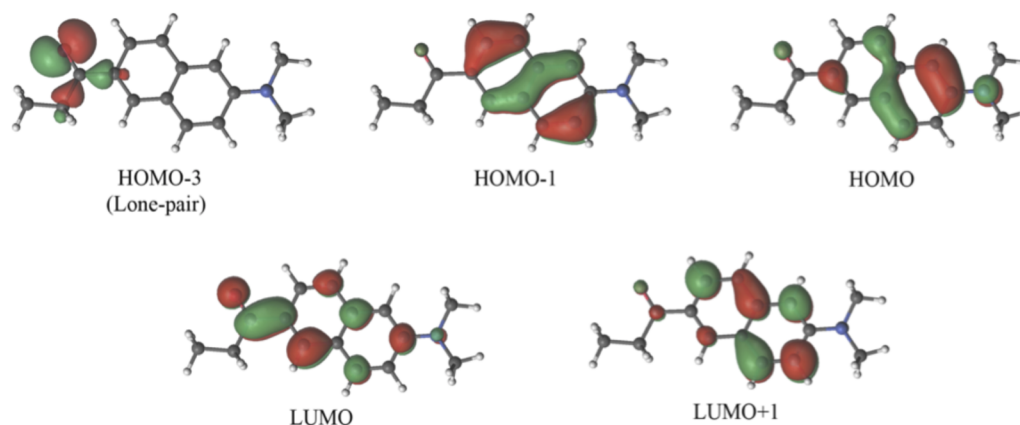


FIG. 4. Molecular orbitals involved in the electron transition of the three lowest excited electronic states: $\pi-\pi^*L_a$ is dominated by HOMO \rightarrow LUMO transition, $\pi-\pi^*L_b$ is dominated by a combination of HOMO \rightarrow LUMO +1 and HOMO -1 \rightarrow LUMO transitions, and $n-\pi^*$ is dominated by HOMO -3 \rightarrow LUMO +1 transition.

TABLE III. Transition energies (in 10^3 cm^{-1}) of Prodan calculated at the CASPT2//CASSCF level in vacuum and in water using PCM and ASEC electrostatic embedding obtained with MC simulations. In boldface, the absorption transition energy (S_0-S_1) and the emission transition energy (S_1-S_0 , S_2-S_0 , and S_3-S_0) were highlighted. The calculated Stokes shift [$\Delta E_1^{\text{cal}}(\text{SS}) = E_1^{\text{cal}} - E_{\text{abs}}^{\text{cal}}$ and $\Delta E_2^{\text{cal}}(\text{SS}) = E_2^{\text{cal}} - E_{\text{abs}}^{\text{cal}}$] is also shown in comparison with the experimental data presented at Table II.

	Vacuum	PCM (water)	ASEC (water)
Franck Condon S_0 geometry			
$\pi-\pi^*L_b$	31.9 S_0-S_1	31.9 S_0-S_2	31.3 S_0-S_2
$n-\pi^*$	32.0 S_0-S_2	33.6 S_0-S_3	31.8 S_0-S_3
$\pi-\pi^*L_a$	34.2 S_0-S_3	30.6 S_0-S_1	30.4 S_0-S_1
$\pi-\pi^*L_b$ equilibrium geometry			
$\pi-\pi^*L_b$	29.7 S_1-S_0	29.3 S_2-S_0	29.3 S_2-S_0
$n-\pi^*$	29.9 S_2-S_0	31.5 S_1-S_0	32.4 S_1-S_0
$\pi-\pi^*L_a$	33.5 S_3-S_0	30.8 S_3-S_0	30.1 S_3-S_0
$n-\pi$ equilibrium geometry			
$n-\pi^*$	22.5 S_2-S_0	24.8 S_3-S_0	21.4 S_3-S_0
$\pi-\pi^*L_b$	30.4 S_1-S_0	30.4 S_2-S_0	31.1 S_2-S_0
$\pi-\pi^*L_a$	31.5 S_3-S_0	27.5 S_1-S_0	36.1 S_1-S_0
$\pi-\pi^*L_a$ equilibrium geometry			
$\pi-\pi^*L_a$	30.6 S_3-S_0	27.3 S_1-S_0	25.3 S_1-S_0
$\pi-\pi^*L_b$	29.2 S_1-S_0	30.3 S_2-S_0	26.0 S_2-S_0
$n-\pi^*$	31.7 S_2-S_0	31.7 S_3-S_0	33.0 S_3-S_0
Stokes shift of high energy			
$\Delta E_1^{\text{cal}}(\text{SS})$	-2.2 S_1-S_0 ($\pi-\pi^*L_b$)	-3.3 S_2-S_0 ($\pi-\pi^*L_a$)	-5.1 S_1-S_0 ($\pi-\pi^*L_a$)
$\Delta E_1^{\text{exp}}(\text{SS})$	-3.6	-8.5	-8.5
Stokes shift of low energy			
$\Delta E_2^{\text{cal}}(\text{SS})$	-9.4 S_2-S_0 ($n-\pi^*$)	-5.8 S_3-S_0 ($n-\pi^*$)	-9.0 S_3-S_0 ($n-\pi^*$)
$\Delta E_2^{\text{exp}}(\text{SS})$	-5.0	-10.3	-10.3

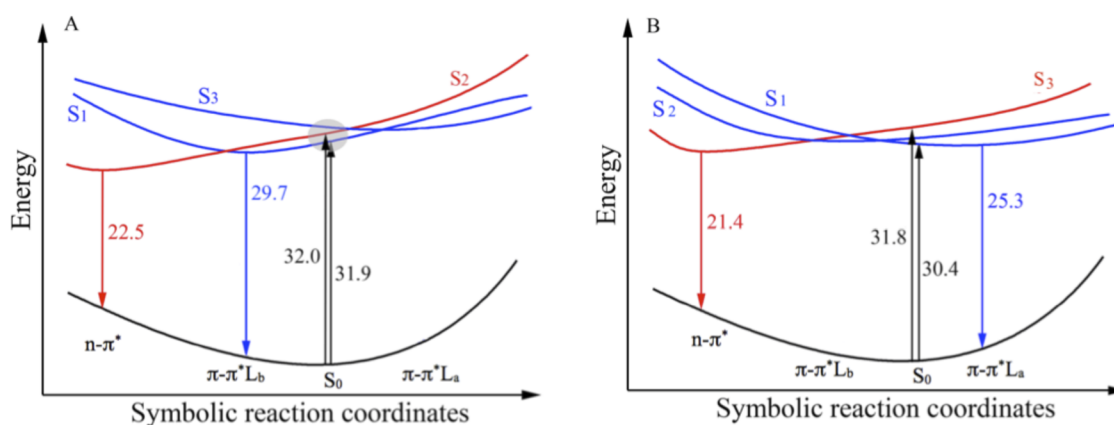


FIG. 5. Schematic representation of the photophysics of the Prodan in vacuum (a) and water (b) using the CASPT2//CASSCF level with the solvent described by the ASEC electrostatic embedding. The energy is the total internal energy corrected by zero-point energy and vibrational entropy. The π - π^* states are represented in blue and the n - π^* state in red. The values (in $\times 10^3 \text{ cm}^{-1}$) were presented in Table III.

These possible internal conversions between excited states of Prodan were not investigated in this work, but it shows clearly that the study of only S_1 state is not enough to describe the complex dual fluorescence of Prodan in solution and even more complex heterogeneous environment such as phospholipid membranes.

The n - π^* state is the lowest excited state at its corresponding equilibrium geometry in vacuum and in water. The calculated emission transition energy $S_3 \rightarrow S_0$ in water is $21.4 \times 10^3 \text{ cm}^{-1}$ that is $4.1 \times 10^3 \text{ cm}^{-1}$ larger than the experimental lower energy emission $E_2^{\text{exp}} = 17.3 \times 10^3 \text{ cm}^{-1}$ in water (see Table II). For the absorption transition energy of the π - π^* L_a state, the calculated value with CASPT2/ASEC method, $E_{\text{abs}}^{\text{cal}} = 30.4 \times 10^3 \text{ cm}^{-1}$, is also overestimated compared with the experimental data, $E_{\text{abs}}^{\text{exp}} = 27.6 \times 10^3 \text{ cm}^{-1}$ (see Table II). Therefore, the calculated Stokes shift of the lower energy $\Delta E_2^{\text{cal}}(\text{SS}) = -9.0$ ($21.4 - 30.4$) $\times 10^3 \text{ cm}^{-1}$ is in good agreement with the experimental value $\Delta E_2^{\text{exp}}(\text{SS}) = -10.3 \times 10^3 \text{ cm}^{-1}$, as shown in Table III.

The S_1 state is the second lowest excited states of Prodan in vacuum and in water. However, in vacuum, it is the π - π^* L_b state, and in water, it changes to the π - π^* L_a state. In water, the calculated emission transition energy $S_1 \rightarrow S_0$ is $25.3 \times 10^3 \text{ cm}^{-1}$. This energy is also overestimated in comparison with the experimental higher energy emission in water, $E_1^{\text{exp}} = 19.1 \times 10^3 \text{ cm}^{-1}$ (see Table II). The calculated value for the Stokes shift of the higher energy is $\Delta E_1^{\text{cal}}(\text{SS}) = -5.1$ ($=25.3 - 30.4$) $\times 10^3 \text{ cm}^{-1}$, in agreement with the experimental Stokes shift in water, $\Delta E_1^{\text{exp}}(\text{SS}) = -8.5 \times 10^3 \text{ cm}^{-1}$, as shown in Table III.

The calculated values for the Stokes shifts of the high and low energies of Prodan in vacuum, $\Delta E_1^{\text{cal}}(\text{SS}) = -2.2 \times 10^3 \text{ cm}^{-1}$ and $\Delta E_2^{\text{cal}}(\text{SS}) = -9.4 \times 10^3 \text{ cm}^{-1}$ (Table III), were compared with the experimental measurements of the absorption transition and the dual fluorescence of Prodan in cyclohexane (Tables II and III), $\Delta E_1^{\text{exp}}(\text{SS}) = -3.6 \times 10^3 \text{ cm}^{-1}$ and $\Delta E_2^{\text{exp}}(\text{SS}) = -5.0 \times 10^3 \text{ cm}^{-1}$. Both Stokes shifts are for the red side and have a qualitative agreement showing a smaller shift for the high energy ΔE_1 than for the low energy, $\Delta E_1(\text{SS}) < \Delta E_2(\text{SS})$. For the low energy Stokes shift $\Delta E_2(\text{SS})$,

our results are overestimated by $-4.4 \times 10^3 \text{ cm}^{-1}$ compared with the experimental data probably because we are not considering the non-equilibrium solvation situation. The non-equilibrium solvation initially describes the situation when the solute is in the excited state, but the solvent molecules did not have enough time to relax their distribution around the solute and followed by the dynamic coupling between the relaxation of the solvent and the solute in the excited state. Usually, calculations on this situation show initially a smaller Stokes shift due to the larger similarity of the solvated ground state and the non-relaxed solvated excited state, but it will dynamically evolve to the equilibrium situation where the solvent will be completely equilibrated with the charge distribution of the excited state relaxed due to the solvent presence. In the case of Prodan in solution, the lifetime decays are large in the nanosecond scale (experimental values¹⁰ of $\tau_1 = 0.2 \text{ ns}$ and $\tau_2 = 0.8 \text{ ns}$ in cyclohexane and between 2.1 ns and 4.5 ns for several solvents, such as chloroform, dichloromethane, acetonitrile, methanol, and water). Therefore, it is expected that the major contributions of the fluorescent emission spectra come from the equilibrium fully relaxed solvation situation. However, this non-equilibrium solvation effect is important and should be considered for a better description of the dual fluorescence of Prodan mostly in low polarity solvents.

In the case of Prodan in water, the Stokes shifts of the high and low energies using the ASEC electrostatic embedding model are $\Delta E_1^{\text{cal}}(\text{SS}) = -5.1 \times 10^3 \text{ cm}^{-1}$ and $\Delta E_2^{\text{cal}}(\text{SS}) = -9.0 \times 10^3 \text{ cm}^{-1}$, showing that the solvent effect is better described by the ASEC than the PCM, $\Delta E_1^{\text{cal}}(\text{SS}) = -3.3 \times 10^3 \text{ cm}^{-1}$ and $\Delta E_2^{\text{cal}}(\text{SS}) = -5.8 \times 10^3 \text{ cm}^{-1}$, as compared with the experimental values, $\Delta E_1^{\text{exp}}(\text{SS}) = -8.5 \times 10^3 \text{ cm}^{-1}$ and $\Delta E_2^{\text{exp}}(\text{SS}) = -10.3 \times 10^3 \text{ cm}^{-1}$. This is mostly due to the good ASEC description of the hydrogen bonds formed between the Prodan and the water molecules. The Stokes shifts of the high energy calculated here [$\Delta E_1^{\text{cal}}(\text{SS}) = -2.2 \times 10^3 \text{ cm}^{-1}$ in vacuum and $\Delta E_1^{\text{cal}}(\text{SS}) = -5.1 \times 10^3 \text{ cm}^{-1}$ in water] are also in agreement with the results obtained by Baral *et al.*⁷² for the high energy of Prodan in hexane, $\Delta E_1^{\text{cal}}(\text{SS}) = -3.3 \times 10^3 \text{ cm}^{-1}$ (-0.41 eV), and in water, $\Delta E_1^{\text{cal}}(\text{SS}) = -9.5 \times 10^3 \text{ cm}^{-1}$ (-1.18 eV). Their results are in

better agreement with the experimental values [$\Delta E_1^{\text{exp}}(\text{SS}) = -3.6 \times 10^3 \text{ cm}^{-1}$ in cyclohexane and $\Delta E_1^{\text{exp}}(\text{SS}) = -8.5 \times 10^3 \text{ cm}^{-1}$ in water]. We are using the MM simulation with the Prodan with rigid geometry, and Baral *et al.*⁷² used flexible Prodan geometry, considering the geometry relaxation due to the solvent interactions. Therefore, it shows that the solvent effect on the geometry relaxation solute is important to the described Stokes shift, but the dual fluorescence can be understood by only analyzing two excited states: the $\pi-\pi^*$ HOMO \rightarrow LUMO S_1 state (high emission energy) and the $n-\pi^*$ HOMO $-3 \rightarrow$ LUMO $+1 S_2$ or S_3 state (low emission energy).

Now, analyzing the dipole moment of the low emission energy state, $\mu_{\text{wat}}(n-\pi^*) = 2.7 \text{ D}$, and the high emission energy state, $\mu_{\text{wat}}(\pi-\pi^* L_a) = 17.2 \text{ D}$ in water and $\mu_{\text{vac}}(\pi-\pi^* L_b) = 5.8 \text{ D}$ in vacuum, it is easy to understand why the high emission state becomes more favorable increasing the solvent polarity. This is a consequence of a much stronger dipole interactions between the solvent molecules and the Prodan at the $\pi-\pi^* L_a$ excited state than at the $n-\pi^*$ excited state.

V. CONCLUSIONS

The absorption spectra of Prodan in water, acetonitrile, dichloromethane, and cyclohexane are well described with different methods (INDO-CIS, TDDFT, and CASPT2), and all agree that the first band is composed of three different electronic transitions: one dark $n-\pi^*$ and two bright $\pi-\pi^*$. It is shown that the two bright excited electronic states can be simultaneously populated in the absorption transitions of Prodan.

Multi-configurational calculations showed that the three excited states, $\pi-\pi^* L_b$, $n-\pi^*$, and $\pi-\pi^* L_a$, are very close to each other in energy at the Franck-Condon geometry, and their equilibrium structures are planar in vacuum. No twist of the carbonyl or dimethylamine groups is observed, and they are in the same plane as the naphthalene rings. Considering the solvent effects in the electronic structure of the solute and in the solvent relaxation around the solute, it was identified that these three excited states can change order depending on the solvent polarity, and following the minimum path energy, internal conversions may occur. The HOMO \rightarrow LUMO S_1 state ($\pi-\pi^* L_b$ in vacuum or $\pi-\pi^* L_a$ in water) relaxes to the equilibrium geometry causing the high emission energy (E_1). The HOMO $-3 \rightarrow$ LUMO $+1 n-\pi^*$ state (S_2 in vacuum or S_3 in water) also relaxes to the equilibrium geometry causing the low emission energy (E_2). The $\pi-\pi^* L_a$ state has a very large dipole moment ($\sim 17 \text{ D}$), and the $n-\pi^*$ state has a very small dipole moment ($\sim 2 \text{ D}$). This information of the larger dipole to the high emission energy E_1 is in agreement with the experimental data that show a larger contribution of E_1 to the emission band in water comparative to cyclohexane. Additionally, the calculated Stokes shifts of the high and low emission energy of Prodan in vacuum and in water are in agreement with the experimental data for cyclohexane and water, respectively.

Hence, our combined experimental and theoretical studies point to a new explanation of the dual fluorescence of molecular probes. We conclude that the Prodan probe does not emit from a solvent-non-relaxed locally excited state and a relaxed twist or planar internal charge transfer excited state. Instead, it fluoresces from two different and independent excited states, first $\pi-\pi^*$ state at high

energy and $n-\pi^*$ state at low energy, which can be populated when Prodan is excited at 340 nm–360 nm. Finally, it should be mentioned that this work focuses on the Prodan molecule, but we contend that the dual fluorescence of the related Laurdan molecule could be understood with the same reasoning.

SUPPLEMENTARY MATERIAL

See the [supplementary material](#) for more information concerning the optimized geometries of Prodan in the ground and first three excited states in vacuum, its polarization using the iterative S-QM/MM procedure and atomic charges, and the solvation structure and additional experimental UV-visible absorption spectra of Prodan in several solvents.

DEDICATION

This paper honors Professor Yvone Primerano Mascarenhas, a pioneer in the field of biomolecular structures in Brazil. With an outstanding capacity for teaching and mentoring, she inspired many students to pursue careers in biophysical chemistry, thus helping in creating important groups.

ACKNOWLEDGMENTS

This work was partially supported by the following Brazilian agencies and projects: FAPESP (Grant No. 2017/11631-2), CAPES for the BioMol Project (Grant No. 23038.004630/2014-35), the National Institute of Science and Technology of Complex Fluids (INCT-FCx) with the CNPq Grant No. 141260/2017-3, and FAPESP (Grant No. 2014/50983-3). C.C.V.-S. acknowledges fellowship support from FAPESP (Grant Nos. 06/55513-9 and 10/08365-0). Y.O.-G. acknowledges fellowship support from FAPESP (Grant No. 12/15161-7). S.C., M.T.L., and K.C. acknowledge financial support from CNPq.

DATA AVAILABILITY

The data that support the findings of this study are available within the article and its [supplementary material](#).

REFERENCES

- ¹G. Weber and F. J. Farris, "Synthesis and spectral properties of a hydrophobic fluorescent-probe: 6-propionyl-2-(dimethylamino)naphthalene," *Biochemistry* **18**, 3075–3078 (1979).
- ²T. Parasassi, F. Conti, and E. Gratton, "Time-resolved fluorescence emission-spectra of laurdan in phospholipid-vesicles by multifrequency phase and modulation fluorometry," *Cell. Mol. Biol.* **32**, 103–108 (1986), see https://www.researchgate.net/profile/Tiziana_Parasassi/publication/19407835_Timeresolved_fluorescence_emission_spectra_of_Laurdan_in_phospholipid-vesicles_by_multifrequency_phase_and_modulation_fluorometry/links/02e7e52a83a68eed4c000000.pdf.
- ³T. Parasassi, G. De Stasio, G. Ravagnan, R. M. Rusch, and E. Gratton, "Quantitation of lipid phases in phospholipid-vesicles by the generalized polarization of Laurdan fluorescence," *Biophys. J.* **60**, 179–189 (1991).
- ⁴F. Moyano, J. J. Silber, and N. M. Correa, "On the investigation of the bilayer functionalities of 1,2-di-oleoyl-sn-glycero-3-phosphatidylcholine (DOPC) large unilamellar vesicles using cationic hemicyanines as optical probes: A wavelength-selective fluorescence approach," *J. Colloid Interface Sci.* **317**, 332–345 (2008).

- ⁵L. A. Bagatolli, B. Maggio, F. Aguilar, C. P. Sotomayor, and G. D. Fidelio, "Laurdan properties in glycosphingolipid-phospholipid mixtures: A comparative fluorescence and calorimetric study," *Biochim. Biophys. Acta, Biomembr.* **1325**, 80–90 (1997).
- ⁶D. Marsh, "Reaction fields in the environment of fluorescent probes: Polarity profiles in membranes," *Biophys. J.* **96**, 2549–2558 (2009).
- ⁷C. C. De Vequi-Suplicy, C. R. Benatti, and M. T. Lamy, "Laurdan in fluid bilayers: Position and structural sensitivity," *J. Fluoresc.* **16**, 431–439 (2006).
- ⁸J. Catalan, P. Perez, J. Laynez, and F. G. Blanco, "Analysis of the solvent effect on the photophysics properties of 6-propionyl-2-(dimethylamino)naphthalene (PRODAN)," *J. Fluoresc.* **1**, 215–223 (1991).
- ⁹J. R. Lakowicz, *Principles of Fluorescence Spectroscopy*, 3rd ed. (Plenum Publishers, New York, 2006).
- ¹⁰C. C. Vequi-Suplicy, R. Coutinho, and M. T. Lamy, "New insights on the fluorescent emission spectra of Prodan and Laurdan," *J. Fluoresc.* **25**, 621–629 (2015).
- ¹¹A. D. Lúcio, C. C. Vequi-Suplicy, R. M. Fernandez, M. T. Lamy, A. D. Lucio, C. C. Vequi-Suplicy, R. M. Fernandez, and M. T. Lamy, "Laurdan spectrum decomposition as a tool for the analysis of surface bilayer structure and polarity: A study with DMPG, peptides and cholesterol," *J. Fluoresc.* **20**, 473–482 (2010).
- ¹²J. R. Lakowicz and A. Balter, "Differential-wavelength deconvolution of time-resolved fluorescence intensities: A new method for the analysis of excited-state processes," *Biophys. Chem.* **16**, 223–240 (1982).
- ¹³J. R. Lakowicz and A. Balter, "Analysis of excited-state processes by phase-modulation fluorescence spectroscopy," *Biophys. Chem.* **16**, 117–132 (1982).
- ¹⁴B. A. Rowe, C. A. Roach, J. Lin, V. Asiago, O. Dmitrenko, S. L. Neal, O. Dmitrenko, S. L. Neal, O. Dmitrenko, and S. L. Neal, "Spectral heterogeneity of PRODAN fluorescence in isotropic solvents revealed by multivariate photokinetic analysis," *J. Phys. Chem. A* **112**, 13402–13412 (2008).
- ¹⁵M. Raguz and J. Brnjac-Kraljević, "Resolved fluorescence emission spectra of PRODAN in ethanol/buffer solvents," *J. Chem. Inf. Model.* **45**, 1636–1640 (2005).
- ¹⁶T. Parasassi, E. K. Krasnowska, L. Bagatolli, and E. Gratton, "Laurdan and Prodan as polarity-sensitive fluorescent membrane probes," *J. Fluoresc.* **8**, 365–373 (1998).
- ¹⁷A. Balter, W. Nowak, W. Pawelkiewicz, A. Kowalczyk, W. Pawelkiewicz, and A. Kowalczyk, "Some remarks on the interpretation of the spectral properties of prodan," *Chem. Phys. Lett.* **143**, 565–570 (1988).
- ¹⁸C. E. Bunker, T. L. Bowen, and Y.-P. Sun, "A photophysical study of solvatochromic probe 6-propionyl-2-(*N,N*-dimethylamino)naphthalene (Prodan) in solution," *Photochem. Photobiol.* **58**, 499–505 (1993).
- ¹⁹B. Mennucci, M. Caricato, F. Ingrosso, C. Cappelli, R. Cammi, J. Tomasi, G. Scalmani, and M. J. Frisch, "How the environment controls absorption and fluorescence spectra of PRODAN: A quantum-mechanical study in homogeneous and heterogeneous media," *J. Phys. Chem. B* **112**, 414–423 (2008).
- ²⁰L. Cwiklik, A. J. A. Aquino, M. Vazdar, P. Jurkiewicz, J. Pittner, M. Hof, and H. Lischka, "Absorption and fluorescence of PRODAN in phospholipid bilayers: A combined quantum mechanics and classical molecular dynamics study," *J. Phys. Chem. A* **115**, 11428–11437 (2011).
- ²¹A. M. Rollinson and H. G. Drickamer, "High-pressure study of luminescence from intramolecular CT compounds," *J. Chem. Phys.* **73**, 5981–5996 (1980).
- ²²W. Nowak, P. Adamczak, A. Balter, and A. Sygula, "On the possibility of fluorescence from twisted intramolecular charge-transfer states of 2-dimethylamino-6-acrylnaphthalenes—A quantum-chemical study," *J. Mol. Struct.: THEOCHEM* **139**, 13–23 (1986).
- ²³R. Adhikary, C. A. Barnes, and J. W. Petrich, "Solvation dynamics of the fluorescent probe PRODAN in heterogeneous environments: Contributions from the locally excited and charge-transferred states," *J. Phys. Chem. B* **113**, 11999–12004 (2009).
- ²⁴Y. P. Morozova, O. M. Zharkova, T. Y. Balakina, and V. Y. Artyukhov, "Effect of proton-donor solvent and structural flexibility of prodan and laurdan molecules on their spectral-luminescent properties," *J. Appl. Spectrosc.* **76**, 312–318 (2009).
- ²⁵R. K. Everett, H. A. A. Nguyen, and C. J. Abelt, "Does PRODAN possess an O-TICT excited state? Synthesis and properties of two constrained derivatives," *J. Phys. Chem. A* **114**, 4946–4950 (2010).
- ²⁶B. N. Davis and C. J. Abelt, "Synthesis and photophysical properties of models for twisted PRODAN and dimethylaminonaphthonitrile," *J. Phys. Chem. A* **109**, 1295–1298 (2005).
- ²⁷V. I. Tomlin, "Nonradiative energy transfer in a concentrated solution of prodan," *Opt. Spectrosc.* **101**, 563–567 (2006).
- ²⁸V. I. Tomlin and K. Hubisz, "Inhomogeneous spectral broadening and the decay kinetics of the luminescence spectra of prodan," *Opt. Spectrosc.* **101**, 98–104 (2006).
- ²⁹M. Novaira, M. A. Biasutti, J. J. Silber, and N. M. Correa, "New insights on the photophysical behavior of PRODAN in anionic and cationic reverse micelles: From which state or states does it emit?," *J. Phys. Chem. B* **111**, 748–759 (2007).
- ³⁰P. Ilich and F. G. Prendergast, "Singlet adiabatic states of solvated PRODAN: A semiempirical molecular orbital study," *J. Phys. Chem.* **93**, 4441–4447 (1989).
- ³¹A. B. J. Parusel, F. W. Schneider, and G. Köhler, "An *ab initio* study on excited and ground state properties of the organic fluorescence probe PRODAN," *J. Mol. Struct.: THEOCHEM* **398-399**, 341–346 (1997).
- ³²M. Viard, J. Gallay, M. Vincent, O. Meyer, B. Robert, and M. Paternostre, "Laurdan solvatochromism: Solvent dielectric relaxation and intramolecular excited-state reaction," *Biophys. J.* **73**, 2221–2234 (1997).
- ³³A. Parusel, "Semiempirical studies of solvent effects on the intramolecular charge transfer of the fluorescence probe PRODAN," *J. Chem. Soc., Faraday Trans. 94*, 2923–2927 (1998).
- ³⁴A. B. J. Parusel, R. Schamschule, and G. Köhler, "Nonlinear optics. A semiempirical study of organic chromophores," *J. Mol. Struct.: THEOCHEM* **544**, 253–261 (2001).
- ³⁵K. A. Kozyra, J. R. Heldt, J. Heldt, M. Engelke, and H. A. Diehl, "Concentration and temperature dependence of Laurdan fluorescence in glycerol," *Z Naturforsch. A* **58**, 581–588 (2003).
- ³⁶B. C. Lobo and C. J. Abelt, "Does PRODAN possess a planar or twisted charge-transfer excited state? Photophysical properties of two PRODAN derivatives," *J. Phys. Chem. A* **107**, 10938–10943 (2003).
- ³⁷M. Novaira, F. Moyano, M. A. Biasutti, J. J. Silber, and N. M. Correa, "An example of how to use AOT reverse micelle interfaces to control a photoinduced intramolecular charge-transfer process," *Langmuir* **24**, 4637–4646 (2008).
- ³⁸A. Samanta and R. W. Fessenden, "Excited state dipole moment of PRODAN as determined from transient dielectric loss measurements," *J. Phys. Chem. A* **104**, 8972–8975 (2000).
- ³⁹K. Coutinho, S. Canuto, and M. C. Zerner, "A Monte Carlo-quantum mechanics study of the solvatochromic shifts of the lowest transition of benzene," *J. Chem. Phys.* **112**, 9874–9880 (2000).
- ⁴⁰W. R. Rocha, K. Coutinho, W. B. De Almeida, and S. Canuto, "An efficient quantum mechanical/molecular mechanics Monte Carlo simulation of liquid water," *Chem. Phys. Lett.* **335**, 127 (2001).
- ⁴¹W. R. Rocha, V. M. Martins, K. Coutinho, and S. Canuto, "Solvent effects on the electronic absorption spectrum of formamide studied by a sequential Monte Carlo/quantum mechanical approach," *Theor. Chem. Acc.* **108**, 31–37 (2002).
- ⁴²S. Miertus, E. Scrocco, and J. Tomasi, "Electrostatic interaction of a solute with a continuum—A direct utilization of *Ab initio* molecular potentials for the prevision of solvent effects," *Chem. Phys.* **55**, 117–129 (1981).
- ⁴³C. C. Vequi-Suplicy, K. Coutinho, and M. T. Lamy, "Electric dipole moments of the fluorescent probes Prodan and Laurdan: Experimental and theoretical evaluations," *Biophys. Rev.* **6**, 63–74 (2014).
- ⁴⁴H. C. Georg, K. Coutinho, and S. Canuto, "Converged electronic polarization of acetone in liquid water and the role in the $n-\pi^*$ transition," *Chem. Phys. Lett.* **429**, 119–123 (2006).
- ⁴⁵R. C. Barreto, K. Coutinho, H. C. Georg, and S. Canuto, "Combined Monte Carlo and quantum mechanics study of the solvatochromism of phenol in water. The origin of the blue shift of the lowest $\pi-\pi^*$ transition," *Phys. Chem. Chem. Phys.* **11**, 1388–1396 (2009).
- ⁴⁶V. Manzoni, M. L. Lyra, R. M. Gester, K. Coutinho, and S. Canuto, "Study of the optical and magnetic properties of pyrimidine in water combining PCM and QM/MM methodologies," *Phys. Chem. Chem. Phys.* **12**, 14023 (2010).
- ⁴⁷K. Coutinho, H. C. Georg, T. L. Fonseca, V. Ludwig, and S. Canuto, "An efficient statistically converged average configuration for solvent effects," *Chem. Phys. Lett.* **437**, 148–152 (2007).

- ⁴⁸C. M. Breneman and K. B. Wiberg, "Determining atom-centered monopoles from molecular electrostatic potentials—The need for high sampling density in formamide conformational-analysis," *J. Comput. Chem.* **11**, 361–373 (1990).
- ⁴⁹N. Ferre and J. G. Angyan, "Approximate electrostatic interaction operator for QM/MM calculations," *Chem. Phys. Lett.* **356**, 331–339 (2002).
- ⁵⁰Y. Orozco-Gonzalez, C. Bistafa, and S. Canuto, "Solvent effect on the Stokes shift and on the nonfluorescent decay of the daidzein molecular system," *J. Phys. Chem. A* **117**, 4404–4411 (2013).
- ⁵¹E. Runge and E. K. U. Gross, "Density-functional theory for time-dependent systems," *Phys. Rev. Lett.* **52**, 997–1000 (1984).
- ⁵²J. Ridley and M. Zerner, "Intermediate neglect of differential overlap technique for spectroscopy: Pyrrole and azines," *Theor. Chim. Acta* **32**, 111–134 (1973).
- ⁵³J. Tomasi, "Thirty years of continuum solvation chemistry: A review, and prospects for the near future," *Theor. Chem. Acc.* **112**, 184–203 (2004).
- ⁵⁴J. Tomasi, B. Mennucci, and R. Cammi, "Quantum mechanical continuum solvation models," *Chem. Rev.* **105**, 2999–3093 (2005).
- ⁵⁵K. Andersson, P. Å. Malmqvist, and B. O. Roos, "Second-order perturbation-theory with a complete active space self-consistent field reference function," *J. Chem. Phys.* **96**, 1218–1226 (1992).
- ⁵⁶F. Aquilante, L. De Vico, N. Ferre, G. Ghigo, P. A. Malmqvist, P. Neogrady, T. B. Pedersen, M. Pitonak, M. Reiher, B. O. Roos, L. Serrano-Andres, M. Urban, V. Veryazov, and R. Lindh, "Software news and update MOLCAS 7: The next generation," *J. Comput. Chem.* **31**, 224–247 (2010).
- ⁵⁷P.-O. Widmark, P.-Å. Malmqvist, and B. O. Roos, "Density matrix averaged atomic natural orbital (ANO) basis sets for correlated molecular wave functions I. First row atoms," *Theor. Chim. Acta* **77**, 291–306 (1990).
- ⁵⁸P.-O. Widmark, B. J. Persson, and B. O. Roos, "Density matrix averaged atomic natural orbital (ANO) basis sets for correlated molecular wave functions II. Second row atoms," *Theor. Chim. Acta* **79**, 419–432 (1991).
- ⁵⁹M. C. Zerner, *ZINDO/UF: A Semi-Empirical Program Package* (University of Florida, Gainesville, USA, 2000).
- ⁶⁰M. J. Frisch, G. W. Trucks, H. B. Schlegel, G. E. Scuseria, M. A. Robb, J. R. Cheeseman, J. A. Montgomery, T. Vreven, Jr., K. N. Kudin, J. C. Burant, J. M. Millam, J. A. Pople *et al.*, GAUSSIAN 03, 2004.
- ⁶¹G. Karlström, R. Lindh, P.-Å. Malmqvist, B. O. Roos, U. Ryde, V. Veryazov, P.-O. Widmark, M. Cossi, B. Schimmelpfennig, P. Neogrady, and L. Seijo, "MOLCAS: A program package for computational chemistry," *Comput. Mater. Sci.* **28**, 222–239 (2003).
- ⁶²M. P. Allen and D. J. Tildesley, *Computer Simulation of Liquids* (Oxford University Press, Oxford, 1989).
- ⁶³W. L. Jorgensen, D. S. Maxwell, and J. Tirado-Rives, "Development and testing of the OPLS all-atom force field on conformational energetics and properties of organic liquids," *J. Am. Chem. Soc.* **118**, 11225–11236 (1996).
- ⁶⁴H. J. C. Berendsen, J. R. Grigera, and T. P. Straatsma, "The missing term in effective pair potentials," *J. Phys. Chem.* **91**, 6269–6271 (1987).
- ⁶⁵H. J. Böhm, I. R. McDonald, and P. A. Madden, "An effective pair potential for liquid acetonitrile," *Mol. Phys.* **49**, 347–360 (1983).
- ⁶⁶W. C. Swope, H. C. Andersen, P. H. Berens, and K. R. Wilson, "A computer simulation method for the calculation of equilibrium constants for the formation of physical clusters of molecules: Application to small water clusters," *J. Chem. Phys.* **76**, 637–649 (1982).
- ⁶⁷H. J. C. Berendsen, J. P. M. Postma, W. F. van Gunsteren, A. Dinola, and J. R. Haak, "Molecular-dynamics with coupling to an external bath," *J. Chem. Phys.* **81**, 3684–3690 (1984).
- ⁶⁸K. Coutinho and S. Canuto, *DICE: A Monte Carlo Program for Molecular Simulation* (University of São Paulo, SP, Brazil, 2009).
- ⁶⁹H. M. Cezar, S. Canuto, and K. Coutinho, "DICE: A Monte Carlo code for molecular simulation including configurational bias Monte Carlo method," *J. Chem. Inf. Model.* **60**, 3472–3488 (2020).
- ⁷⁰J. W. Ponder and F. M. Richards, "An efficient Newton-like method for molecular mechanics energy minimization of large molecules," *J. Comput. Chem.* **8**, 1016–1024 (1987).
- ⁷¹C. E. Kundrot, J. W. Ponder, and F. M. Richards, "Algorithms for calculating excluded volume and its derivatives as a function of molecular-conformation and their use in energy minimization," *J. Comput. Chem.* **12**, 402–409 (1991).
- ⁷²S. Baral, M. Phillips, H. Yan, J. Avenso, L. Gundlach, B. Baumeier, and E. Lyman, "Ultrafast formation of the charge transfer state of prodan reveals unique aspect of the chromophore environment," *J. Phys. Chem. B* **124**, 2643–2651 (2020).
- ⁷³H. C. Georg, K. Coutinho, and S. Canuto, "Solvent effects on the UV-visible absorption spectrum of benzophenone in water: A combined Monte Carlo quantum mechanics study including solute polarization," *J. Chem. Phys.* **126**, 034507 (2007).
- ⁷⁴S. Canuto, K. Coutinho, and D. Trzesniak, "New developments in Monte Carlo/quantum mechanics methodology. The solvatochromism of beta-carotene in different solvents," *Adv. Quantum Chem.* **41**, 161–183 (2002).
- ⁷⁵Y. Huang, X.-Y. Li, K.-X. Fu, and Q. Zhu, "New formulation for non-equilibrium solvation: Spectral shifts and cavity radii of 6-propanoyl-2(*N*, *N*-dimethylamino) naphthalene and 4-(*N*, *N*-dimethylamino) benzonitrile," *J. Theor. Comput. Chem.* **05**, 355–374 (2006).